Influence of Strut Radius and Relative Density of Lattice Structures used as Sandwich Panels' Core

Diogo Miguel Rosa Pereira
diogo.rosa.pereira@tecnico.ulisboa.pt

Instituto Superior Técnico, Universidade de Lisboa, Portugal

January 2021

Abstract

Sandwich panels with truss or lattice cores are an alternative to the conventional honeycomb core design. This is because the truss core leads to a lower weight while maintaining the same levels of strength, stiffness and energy absorption as the honeycomb core. The main purpose of this research is to investigate how the variation of truss radius and relative density of the unit cell used in the core influences the flexural behavior of sandwich panels. Previously, Monteiro et al [1] made a study on the effects that lattice topology had on the flexural behavior of sandwich panels. He used various topologies inspired on the crystalline structure of atoms and concluded that body and face centred with z-axis struts (BFCZ) provided the best flexural behavior. So, this was the lattice topology chosen. This unit cell topology was tested with radius of 0.8 mm, 0.92 mm and 1.1 mm in combination with the relative density values of 0.35, 0.3 and 0.25. In sum, a total of nine different core units and consequently nine different sandwich panels were studied. Numerical and experimental analysis were used to evaluate the flexural behavior of the nine structures under three-point bending tests. For the numerical analysis, a finite element software Siemens NX was used. Fused deposition modelling (FDM) also denoted by Fused Filament Fabrication (FFF) was used to print poly-lactic neutral acid samples with the different configurations mentioned. The sandwich panels that were manufactured consist in a lattice core made by repetitions of the unit cell and by two thin plates, one above and the other below the core, that were manufactured together. The results obtained led to the conclusion that a decrease of relative density would result in improved strength and stiffness of the structures. It was also found that a variation of radius would result in different properties depending on the relative density. When increasing the radius of lattices with low relative density (0.25), the overall performance would be worse because there would be a minimum value of the strength and stiffness. However the same variation of radius in lattices with high values of relative density (0.35) leads to the appearance of a maximum value of strength and stiffness.
Keywords: Sandwich panels, lattice structures, three-point bending test, numerical simulation, fused deposition method

1. Introduction

Sandwich panels were created in the 1940s and can be manufactured in many different materials as just about any thin plate material can be used to manufacture these panels. In the beginning, the cores of these panels were 2D structures, specially hexagonal honeycomb structures, but later 3D structures and materials, such as foams, were introduced as core materials. Besides the core, a sandwich panel is constituted by two face sheets, one above and the other below the core, as can be seen in figure 1. Sandwich panels have great structural characteristics, as despite their low weight, they have great strength, stiffness and are capable of great energy absorption.

There are three types of 3D structures: ceramics, metal and polymers. These types of structures

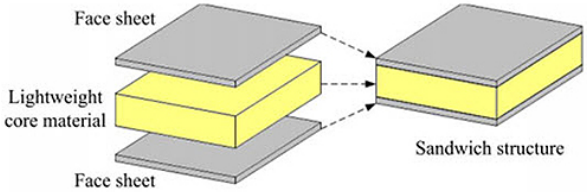

Figure 1: Example of a sandwich panel [2]

are formed by extending the properties of the base material. This repetition of the properties will result improved properties instead of the same properties of the base material. The most important factors that influence the overall properties of the cellular structure are the properties of the base solid, the topology and shape of the cell edges and faces, and the relative density of the cell [3].

Because of the advent of AM methods, a new type of 3D structure could be manufactured. These structure are the lattice structures. A lattice structure is formed by the repetition of a basic unit cell unit, formed by struts or small sheet panels. Because of the freedom of the manufacture provided by the AM methods, 3D printed lattice structures are being used in various fields and objects, since sports goods to construction and even arts [4]. This happens because not only because the 3D printed lattice structures have all the advantages of the cellular solids but they can also be specially tailored to fit its function, through the use of topology optimization. As such, various studies with the aim of developing 3D printed lattice structures for specific uses have been developed. There are a wide variety of studies with many different focuses, such as on the materials used [5, 6] or the geometry of the core [1, 7, 8]. All the studies mentioned compare the strength, stiffness and energy absorption to the regular sandwich panel whit an hexagonal honeycomb core and concluded that with the correct unit cell arrangement of the core, the structures studied could surpass the performance of this classic sandwich panel. In the Lab2ProD, Monteiro et al [1] developed a study on the performance of 3D printed sandwich panels with a core made of lattice structures. These lattice structures had various different unit cell geometry but all had the same relative density. They used five different lattice structures inspired on atomic arrangements such as Body Centred (BC), Body Centred with z axis struts (BCZ), Body and Face Centred with z axis struts (BCFZ), Face Centred with z axis struts (FCZ) and Parallelepipedic Simple (PS). Along with these structures, an hexagonal honeycomb with the same relative density was also manufactured in order to draw comparisons. All these geometries can be observed in figure 2 [1].

From all the lattice unit cells studied, Monteiro et al [1] concluded that the BCFZ unit cell had the best overall properties when used as a core of sandwich panel. The objective of this study is to design, produce and analyse the stiffness, strength and energy absorption of nine sandwich panels, differing in core geometry. Despite the geometry of the unit cell always being the BCFZ geometry, each specimen will have a different combination of radius and relative density. In order to have the nine different combinations of radius and relative density, the values of radius used were 0.8 mm, 0.92 mm and 1.1 mm and the values of relative density used were 0.35, 0.3 and 0.25. To meet these goals, the following step must be achieved: design nine unit cell beam structures (sandwich panels) with approximately similar length and width. A Finite Element Analysis (FEA) study was developed

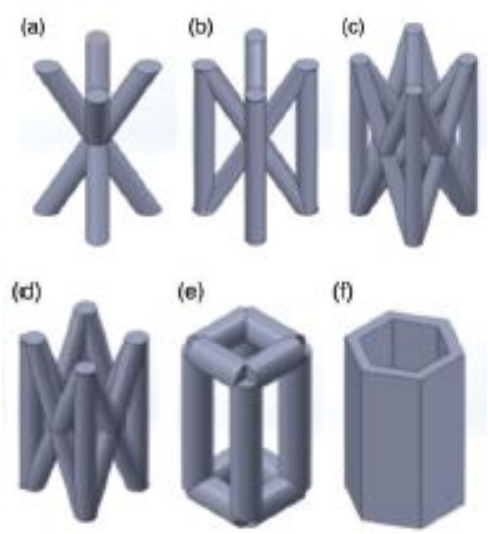

Figure 2: Lattice Unit Cells studied by Monteiro: (a) body centred (BC), (b) body centred with z axis struts (BCZ), (c) body and face centred with z axis struts (BCFZ), (d) face centred with z axis struts (FCZ), (e) parallelepipedic simple (PS) and (f) hexagonal honeycomb cell (HEX) [1]

for each of the sandwich panels subjected to a three point bending test. Samples were produced using the FDM process in a commercial printing machine. Experimental tests of all the sandwich panels subjected to three point bending test, compare the structures in terms of load-displacement curves, rigidity and absorbed energy with each other and compare the results of the FEA with the experimental results.

2. Materials and Methods

The specimens were all manufactured using neutral polylactic acid (PLA-N), which a derived from the base polylactic acid (PLA). Both of them are thermoplastic polymers that are commonly produced form fermented plant starch. Both are semi-biodegradable (both become innocuous acid) and so are used various fields from food packaging to medical prostheses. The PLA-N is an improved version of the PLA created to support larger loads. The manufacturer of the spools used in this study indicates that this variant of the PLA has 27,5% more torsional strength and 12,5% more flexural strength than the base material [9].

2.1. Specimens Design

The nine different unit cells were designed using the CAD software Solidworks 2018. During the design process, it was decided that unit cells with the same radius would have the same base dimensions (length and width). The dimensions of the nine unit cells are presented in table 1. It is important to mention that due to the limitations of printer available, exact values of relative density could not be reached, but a good approximate values was

obtained. The nine unit cells designed are presented from figures 3 to 11.

Figure 3: Unit Cell 1

Figure 4: Unit Cell 2

Figure 5: Unit Cell 3

Figure 6: Unit Cell 4

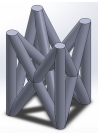

Figure 7: Unit Cell 5

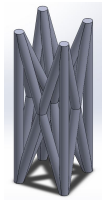

Figure 8: Unit Cell 6

Figure 9: Unit Cell 7

Figure 10: Unit Cell 8

Figure 11: Unit Cell 9

Having designed all of the unit cells, it is now possible to design the sandwich panels. The core is created by repeating the unit cell in the length and width direction. In his study, Monteiro et al [1] designed the top and bottom plates with a thickness of 1.25 mm. The other dimensions of the plate were dependent on the dimensions of the core, as the plates were designed with an extra 0.5 mm in each edge so that there is some extra space between the outer edges of the core and the edges of the plate [1]. In order to maintain uniformity, the same design specifications will be used in the design of plates. The final dimensions of the nine different plates and the number of repetitions used in the core on the length and width direction is presented in table 2. Figure 12 shows one of the sandwich panels designed for this study.

2.2. Specimens Manufacture

Three copies of each specimens were manufactured using FDM technology, which results in a total of 27 manufactured specimens. The 3D printer used was an Ultimaker3. All the prints were made with an infill percentage of 100% and without the use of supports. As it is normal in the FDM manufacturing process, the model was designed with the assistance of a CAD software, which in this case was Solidworks 2018. The design is then exported as a Standard Triangle Language (STL) file into a slicer software. The slicer software used was CURA fromm Ultimaker which slices the model into layers and generates the G-code that the machine then reads and uses to make the print. This G-code file contains the path for the extrusion head from the printer to follow. Figure 13 shows the Ultimaker3 device during the manufacture of two samples. Although the option of printing two specimen at the same time is not recommended as it is more prone to printing defects, in this case it was sometimes used without problems arising. In other prints, there were some major printing failures, such as lack of adhesion to the building plate or layer shifts which led to reprints of some specimens. Some minor defects like stringing were also detected but were not considered compromising to this study.

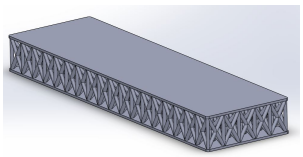

Figure 12: One of the nine sandwich panels designed for this study

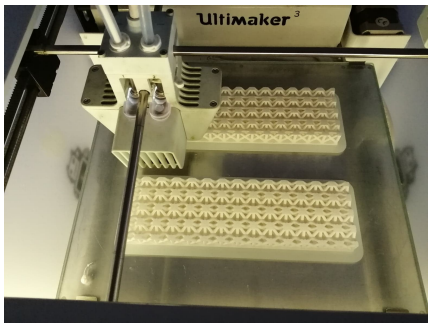

Figure 13: Ultimaker 3 during the printing process

2.3. Experimental Process

The twenty seven specimens were manufactured to be subjected to 3PB tests. Before these tests, all the specimens were measured and weighted. These measurements are summarized in table 3.

The 3PB were performed according to the standart ASTM C393-00 (Standard Test Method for Flexural Properties of Sandwich Constructions) [10]. Figure 14 presents a scheme of the three-point bending test where L_1 is the midspan distance, which the distance between the two bottom rollers. The distance between the bottom roller and the edge of the sandwich panels is the overhang distance. In this type of test is desirable that the rollers are exerting force in the struts. Because the unit cells had different base dimensions and the number of repetitions for each specimen was

Table 1: Dimensions of the nine different unit cells designed

Unit Core	Radius (mm)	ρ_{Rel}	Base Dimensions (mm)	Height (mm)
1	0.8	0.35	10	10
2	0.8	0.30	10	14.5
3	0.8	0.25	10	28.5
4	0.92	0.35	11.5	11.5
5	0.92	0.30	11.5	16.5
6	0.92	0.25	11.5	33
7	1.1	0.35	14	14
8	1.1	0.30	14	17.5
9	1.1	0.25	14	29

Table 2: Dimensions and number of cell repetitions of the nine different sandwich panels designed

Specimen	Radius of Core Structure (mm)	Relative Density of the Core Basic Unit	Length (mm)	Width (mm)	Thickness (mm)	Cell Repetitions Lengthwise	Cell Repetitions Widthwise
1	0.8	0.35	170.6	53	12.5	20	6
2	0.8	0.3	170.6	53	17	20	6
3	0.8	0.25	170.6	53	31.5	20	6
4	0.92	0.35	176.7	51.1	14	18	5
5	0.92	0.3	176.7	51.1	19	18	5
6	0.92	0.25	176.7	51.1	35.5	18	5
7	1.1	0.35	168.4	50.4	16.5	14	4
8	1.1	0.3	168.4	50.4	20	14	4
9	1.1	0.25	168.4	50.4	31.5	14	4

different, the midspan and overhang distances had to be different for each specimen. The midspan distance were 140 mm for the specimens 1, 2 and 3, resulting in an overhang of 30 mm; 138 mm for the specimens 4, 5 and 6, resulting in an overhang of 34.5 mm; 140 mm for the specimens 7, 8 and 9, resulting in an overhang of 28 mm. Figure 15 presents the experimental set-up prior to the beginning of the test.

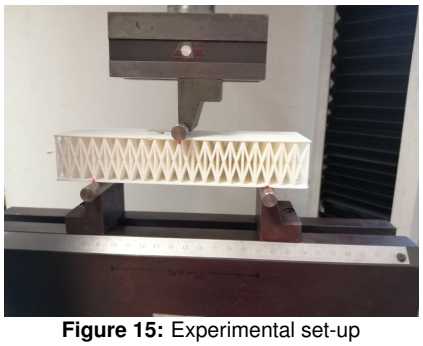

Figure 15: Experimental set-up

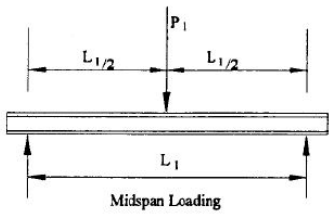

Figure 14: Loading diagram of a 3PB test

The equipment used for all the experimental process was an Instron 3369 with a 50 kN load cell, with the top roller moving at $2.5mm/min$. This equipment is presented in figure 16. The load-displacement data from the procedures were obtained using the Bluehill software.

2.4. Numerical Simulation

The numerical simulation made for this work was executed with the software Siemens NX, version 1915. This software uses the Finite Element Method (FEM) to do its calculations. In order to proceed to all the calculations necessary, this software needs three different files: a part file, a fem file and a sim file. When all these files are ready, a solution solver to define the parameters of the solution is needed. Figure 17 presents the part file, the fem file and the sim file, respectively. A mesh refinement study was made to improve the degree of certainty of the results obtained without the increase of the processing time. The convergence criterion was defined as less than 5% changes in the maximum von Misses stress registered in the top skin.

Table 3: Dimensions and weight of the twenty seven sandwich panels that were subjected to a 3PB test

Specimen	Length (mm)	Width (mm)	Thickness (mm)	Weight (g)
1.1	170.2	52.80	12.40	49.458
1.2	170.2	53.08	12.32	51.093
1.3	170.0	52.86	12.32	50.683
2.1	170.8	53.07	16.85	58.689
2.2	170.6	53.15	16.78	57.138
2.3	171.0	52.98	16.89	57.196
3.1	170.8	52.69	31.40	80.698
3.2	170.3	52.71	31.35	84.766
3.3	170.2	52.70	31.27	83.872
4.1	176.8	51.12	14.12	52.273
4.2	176.7	51.19	14.17	52.343
4.3	177.8	51.04	13.38	50.823
5.1	177.0	51.39	18.91	61.715
5.2	176.8	51.21	18.79	60.601
5.3	176.5	51.04	18.70	61.738
6.1	176.5	50.82	32.26	58.318
6.2	176.7	50.80	35.20	97.320
6.3	176.2	50.21	16.58	56.678
7.1	168.4	50.15	16.42	58.318
7.2	168.9	50.18	19.75	63.431
7.3	168.6	50.21	16.58	56.678
8.1	168.5	50.11	19.93	62.503
8.2	168.8	50.18	19.75	63.431
8.3	168.3	50.44	19.93	64.526
9.1	168.5	50.08	31.15	83.459
9.2	168.1	50.11	31.42	85.154
9.3	168.1	50.08	31.40	84.279

Figure 16: Instron 3369 - the equipment used for all the 3PB tests

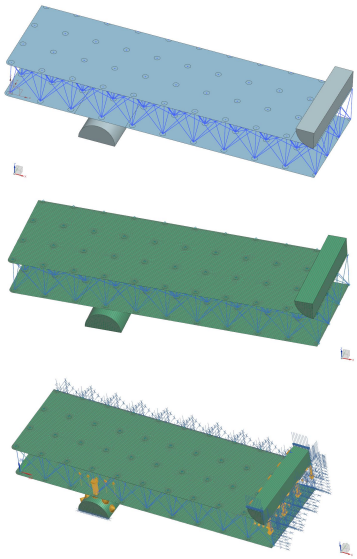

Figure 17: Files used by the software to perform the numerical simulation

3. Results and Discussion

3.1. Numerical Simulation

The numerical simulation is based in a linear elastic analysis made in Siemens NX. From figures 18 to 26 the results of the FEA analysis of all the structures analysed are shown. In particular, it is displayed the elemental von Misses stresses in the skins.

Figure 27 shows the load-displacement curves for all the specimens until a displacement of 4 mm. Using these curves, it is possible to calculate the maximum load, stiffness and energy absorption for all the specimens. These results along with the maximum von Misses stress registered in the top skin of each specimen are presented in tables 4 and 5. In table 4 the results are grouped by strut

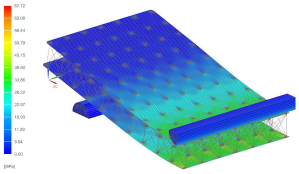

Figure 18: FEA of specimen 1

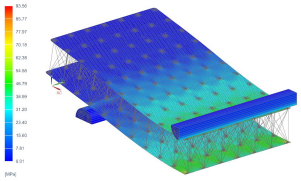

Figure 19: FEA of specimen 2

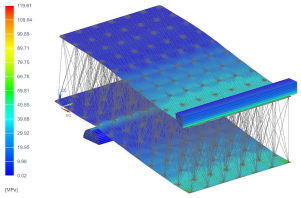

Figure 20: FEA of specimen 3

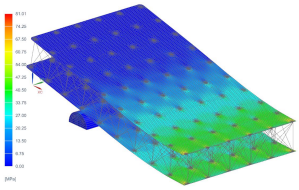

Figure 21: FEA of specimen 4

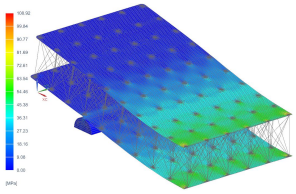

Figure 22: FEA of specimen 5

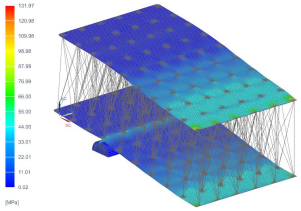

Figure 23: FEA of specimen 6

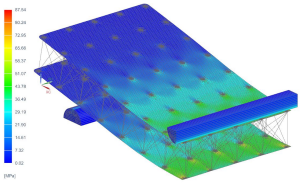

Figure 24: FEA of specimen 7

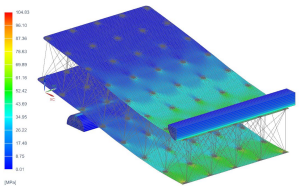

Figure 25: FEA of specimen 8

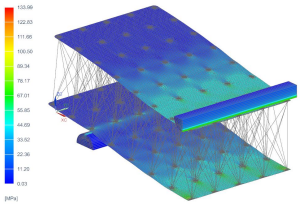

Figure 26: FEA of specimen 9

radius in order to compare the effects of the relative density. In table 5 the results are grouped by relative density in order to compare the effects of the strut radius.

Observing first the table 4, we can see that the numerical simulation points to the fact that a decrease of the relative density leads to a better performance of the specimen in all the studied parameters. But there is a trade-off because decreasing the relative density will lead to higher thickness and so higher production times.

Observing now the table 5, we can see that an increase of the radius leads to a better performance of the specimen in all the studied parameters. Again, the same trade-off regarding the production time must be consider, as an increase of radius leads to higher production times.

3.2. Experimental Tests

From the data provided by the Bluehill software, it was possible to plot load-displacement curves for all the specimens. Using these curves, the load at fracture, displacement at fracture, initial stiffness (slope of the linear region) and energy absorbed were calculated for all the specimens tested. The results are presented at table 6.

After testing all the specimens, it was noticed that the specimens had three distinct primary fracture modes. The first fracture mode (Mode 1) was

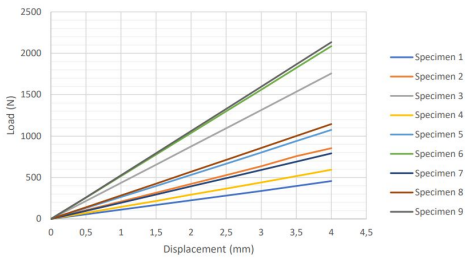

Figure 27: Numerical load-displacement curves of the nine specimens analysed

Table 4: FEA results, where the specimens are grouped by radius

Specimen	Radius (mm)	Relative Density	Applied Force in top Roller (N)	Maximum σ_{VM} in top Skin (MPa)	Stiffness K (N/mm)	Absorbed Energy (J)
1	0.8	0.35	457.08	67.72	114.27	0.91
2		0.3	853.97	93.56	213.49	1.71
3		0.25	1756.97	119.61	439.24	3.51
4	0.92	0.35	594.19	81.01	148.35	1.19
5		0.3	1075.21	108.92	268.86	2.15
6		0.25	2086.16	131.97	521.77	4.17
7	1.1	0.35	791.78	87.54	197.95	1.58
8		0.3	1145.40	104.83	286.35	2.29
9		0.25	2133.77	133.99	533.44	4.27

Table 5: FEA results, where the specimens are grouped by relative density

Specimen	Relative Density	Radius (mm)	Applied Force in top Roller (N)	Maximum σ_{VM} in top Skin (MPa)	Stiffness K (N/mm)	Absorbed Energy (J)
1	0.35	0.8	457.08	67.72	114.27	0.91
4		0.92	594.186	81.01	148.35	1.19
7		1.1	791.78	87.54	197.95	1.58
2	0.3	0.8	853.97	93.56	213.49	1.71
5		0.92	1075.21	108.92	268.86	2.15
8		1.1	1145.40	104.83	286.35	2.29
3	0.25	0.8	1756.97	119.61	439.24	3.51
6		0.92	2086.16	131.97	521.77	4.17
9		1.1	2133.77	133.99	533.44	4.27

characterized by the failure of the struts. In this fracture mode, the struts fail under pressure but tend to return to their original position (touching but not connected to each other) once the pressure is alleviated. So, the fracture of the struts is not easily perceptible without the pressure. The second fracture mode (Mode 2) was characterized by failure in the connection between the struts and the top skin. It is important to mention that in this failure mode there was not any failure between the struts and the bottom skin. Finally, the third and last fracture mode (Mode 3) is a mixed fracture mode, where none of the previously mentioned fracture modes were dominant. The specimens that fractured according to this mixed fracture mode had a total rupture of struts and skins in its mid-plane, just below where the top roller of the 3PB test was positioned. In table 6, is presented the fracture mode of each of the different specimens tested. The three different fracture modes can be observed in figure 28.

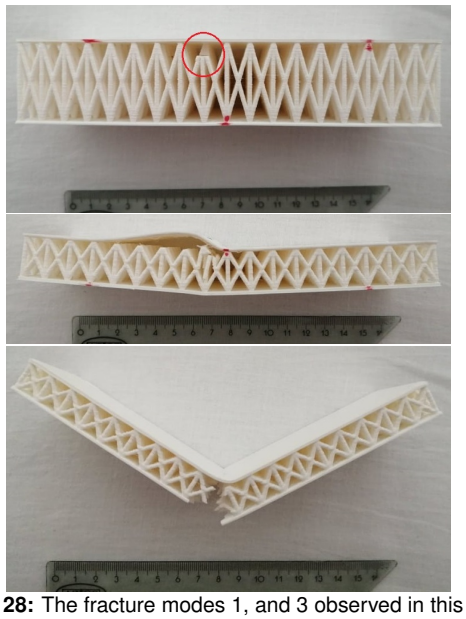

Figure 28: The fracture modes 1, and 3 observed in this study, respectively

3.3. Comparison between methods

Observing all the specimens after the 3PB, along with the small plastic section existent in all the load-displacement curves, we can conclude that all the specimen have a brittle fracture. So, a linear elastic numerical analysis is the best method compare with the experimental work. In order to have a valid comparison, the numerical simulations were remade with the average displacement from table 6 applied to the respective specimen. The comparison between the methods can be done with the help of tables 7 and 8. These tables show the results and properties calculated from the new numerical simulations made with the new displacements and the average values from table 6.

Table 6: Experimental results, specifically the force applied to the top roller, the stiffness and the energy absorbed by the specimens until the fracture. Also presented is the failure mode of each specimen

Specimen	Displacement (mm)	Maximum Load (N)	Stiffness K (N/mm)	Energy Absorbed (J)	Fracture Mode
1.1	5.68	674.19	182.16	2.43	3
1.2	6.23	746.13	183.47	2.88	3
1.3	5.85	690.68	177.08	2.55	2
Average 1	5.92 ± 0.15	703.67 ± 21.23	180.90 ± 1.91	2.62 ± 0.13	
2.1	4.11	817.83	286.12	2.10	1
2.2	5.75	909.28	270.48	3.33	1
2.3	3.97	734.55	266.51	1.79	1
Average 2	4.61 ± 0.57	820.55 ± 44.36	274.34 ± 5.88	2.42 ± 0.47	
3.1	2.86	855.77	402.63	1.48	1
3.2	1.98	820.01	465.91	0.89	1
3.3	2.23	797.37	457.46	1.02	2
Average 3	2.36 ± 0.26	824.38 ± 15.69	442.00 ± 19.69	1.13± 0.17	
4.1	4.97	528.48	173.65	1.71	3
4.2	4.94	514.41	179.83	1.72	3
4.3	4.01	525.26	165.79	1.22	2
Average 4	4.64 ± 0.31	522.72 ± 4.15	173.09 ± 3.65	1.55 ± 0.16	
5.1	4.02	1012.87	367.49	2.54	2
5.2	3.84	1000.33	360.77	2.33	2
5.3	3.54	1021.74	376.26	2.11	2
Average 5	3.80 ± 0.13	1011.65 ± 5.66	368.17 ± 4.04	2.33 ± 0.11	
6.1	2.07	1326.36	807.89	1.59	1
6.2	1.89	1305.22	831.18	1.40	1
6.3	1.64	1165.56	814.22	1.05	1
Average 6	1.87 ± 0.11	1265.71 ± 50.08	817.76 ± 6.71	1.34 ± 0.15	
7.1	4.88	921.03	301.77	2.94	3
7.2	3.45	858.58	304.16	1.65	3
7.3	3.04	825.48	303.76	1.35	2
Average 7	3.79 ± 0.54	868.36 ± 26.33	303.23 ± 0.72	1.98 ± 0.48	
8.1	2.47	850.73	385.44	1.10	1
8.2	2.95	1032.90	425.83	1.69	1
8.3	3.21	1081.00	417.44	1.91	1
Average 8	2.88 ± 0.20	988.21 ± 68.74	409.60 ± 12.06	1.57 ± 0.24	
9.1	1.70	1171.15	722.98	1.03	2
9.2	1.97	1289.35	784.48	1.45	2
9.3	1.90	1055.66	741.98	1.20	2
Average 9	1.86 ± 0.08	1172.05 ± 58.65	749.81 ± 17.33	1.23 ± 0.11	

Table 7: Comparison between the methods, where the specimens are grouped by radius

Specimen	d Fail (mm)	Load Num (N)	Load Exp (N)	K Num (N/mm)	K Exp (N/mm)	E_{abs} Num (J)	E_{abs} Exp (J)
1	5.92	680.08	703.67	114.27	180.90	2.01	2.62
2	4.61	987.63	820.55	213.49	274.37	2.27	2.42
3	2.36	1032.56	824.38	439.24	442.00	1.22	1.13
4	4.64	691.09	522.72	148.35	173.09	1.60	1.55
5	3.80	1023.08	1011.65	268.86	368.17	1.94	2.33
6	1.84	951.90	1265.71	521.77	817.76	0.87	1.34
7	3.79	749.90	868.36	197.95	303.23	1.42	1.98
8	2.88	821.64	988.21	286.35	409.57	1.18	1.57
9	1.86	984.12	1172.05	280.94	749.81	0.91	1.23

Table 8: Comparison between the methods, where the specimens are grouped by relative density

Specimen	d Fail (mm)	Load Num (N)	Load Exp (N)	*K* Num (N/mm)	*K* Exp (N/mm)	E_{abs} Num (J)	E_{abs} Exp (J)
1	5.92	680.08	703.67	114.27	180.90	2.01	2.62
4	4.64	691.09	522.72	148.35	173.09	1.60	1.55
7	3.79	749.90	868.36	197.95	303.23	1.42	1.98
2	4.61	987.63	820.55	213.49	274.37	2.27	2.42
5	3.80	1023.08	1011.65	268.86	368.17	1.94	2.33
8	2.88	821.64	988.21	286.35	409.57	1.18	1.57
3	2.36	1032.56	824.38	439.24	442.00	1.22	1.13
6	1.84	951.90	1265.71	521.77	817.76	0.87	1.34
9	1.86	984.12	1172.05	280.94	749.81	0.91	1.23

Comparing first the results for specimens with the same strut radius but different relative densities, interesting conclusions arise. To do this comparison, one should use the table 7 as the specimens there are grouped by strut radius (specimens 1, 2 and 3 have a strut radius of 0.8 mm; specimens 4, 5 and 6 have strut a radius of 0.92 mm; specimens 7, 8 and 9 have strut a radius of 1.1 mm). Contrary to what was predicted by the numerical simulations, the experimental results suggest that a decrease in relative density does not equate to a better performance for all the parameters. Although, the experimental results almost totally agree in the numerical results regarding the influence of the relative density in the maximum load supported and stiffness of the specimen, with only the numerical load of the specimen 6 and the numerical stiffness of the specimen 9 disagreeing with this conclusion. Regarding the energy absorption, the experimental results do not provide any trend, which suggests that for each specific strut radius there will be an optimal value of relative density which will provide a maximum of energy absorption.

Comparing now the results for specimens with the same relative density but different strut radius. One should use the table 8 as the specimens there are grouped by their relative density (specimens 1, 4 and 7 have a relative density of 0.25; specimens 2, 5 and 8 have a relative density of 0.3; specimens 3, 6 and 9 have strut a relative density of 0.25). Specimens with a relative density of 0.35 (specimens 1, 4 and 7) seem to have a minimum value to the measured parameters, which is dependent on the radius. This is concluded because all of the parameters decrease when increasing the radius from to 0.8 mm to 0.92 mm but then all increase when the radius increases from 0.92 mm to 1.1 mm. The contrary can be said for the specimens with relative densities of 0.25. In this case, the measured parameters increase when increasing the radius from to 0.8 mm to 0.92 mm and then decrease when the radius increases from 0.92 mm to 1.1 mm, which is consistent with the numerical simulations. Finally, no clear pattern can be found for the specimens with a relative density of 0.3. This suggest that all the specimens have an optimal strut radius that is dependent from their relative density.

4. Conclusions and Future Work

In this study, nine sandwich panels were designed with a unit cell inspired by the crystalline structures with cubic arrangements. The unit cell used was a Body and Face Centered Unit Cell with z-struts.The differences between the nine unit cells and consequently between the sandwich panels, were the radius of the struts and the relative density of the unit cell. Experimental tests and numerical simulations were used to analyse the mechanical response and failure behaviour of all the cores when a three-point bending load was applied.

For the most part, an agreement was found between the data obtained of the experimental tests and of the FEA. The experimental tests for all the specimens showed that the failure occurs in the top skin.This is consistent with the data gathered form the numerical simulations, which stated that the higher von Misses stresses occurred in the top skin.

As two parameters were varied for this study, we must analyse the effects of the variation individually. Comparing the results of the variation of the relative density for structures with the same strut radius, the experimental results and numerical simulations point to the conclusion that a decrease of the relative density would lead to higher strength and stiffness. Comparing now the results of the variation of the radius of the struts for structures with the same relative density, there is a disagreement between numerical and experimental results. The numerical results suggest that there is an optimal value of strut radius for each relative density that would results in optimal values strength, stiffness and energy absorption. On the other hand, the experimental results are more dispersed. These results suggest that at higher values of rel-

ative density there is a strut radius that results in minimum value of strength and stiffness. However, at lower values of relative density,there is a strut radius that results in maximum value of strength and stiffness. This leads to the conclusion the effects of the variation of the strut radius are different for different values of relative density.

Future work on this topic should consist in the search for new lattice topology and the improvement of the BCFZ topology used in order to create a structures that surpass the properties of the conventional hexagonal honeycomb structure. This could be achieved through the use of a topology optimization study in conjunction with the use of FDM to manufacture the structures. Due to the different failure modes encountered during this study, a future work made to develop of a failure map to predict the failure mode depending on the characteristic of the structures. Finally, in order to create more approximate numerical simulations, a future work on the influence of the simplification of the numerical simulations should be conducted.

References

[1] JG Monteiro, M Sardinha, F Alves, AR Ribeiro, L Reis, AM Deus, M Leite, and M Fátima Vaz. Evaluation of the effect of core lattice topology on the properties of sandwich panels produced by additive manufacturing. *Proceedings of the Institution of Mechanical Engineers, Part L: Journal of Materials: Design and Applications*, page 1464420720958015, 2020.

[2] TotalMateria. Sandwich steel panels: Part one. in: Total Materia Website (2017), https://www.totalmateria.com/page.aspx?ID=CheckArticlesite=ktsLN=PTNM=484 Accessed: 2020-12-08.

[3] Michael F Ashby. The properties of foams and lattices. *Philosophical Transactions of the Royal Society A: Mathematical, Physical and Engineering Sciences*, 364(1838):15–30, 2006.

[4] Branch techonology. in: Branch Techonology Website (2020), https://www.branch.technology/ Accessed 2020-12-09.

[5] Y Li, H Jahr, P Pavanram, FSL Bobbert, U Puggi, X-Y Zhang, B Pouran, MA Leeflang, H Weinans, J Zhou, et al. Additively manufactured functionally graded biodegradable porous iron. *Acta biomaterialia*, 96:646–661, 2019.

[6] Maciej Mazur, Martin Leary, Matthew McMillan, Joe Elambasseril, and Milan Brandt. Slm additive manufacture of h13 tool steel with conformal cooling and structural lattices. *Rapid Prototyping Journal*, 2016.

[7] J Kadkhodapour, H Montazerian, A Ch Darabi, AP Anaraki, SM Ahmadi, AA Zadpoor, and S Schmauder. Failure mechanisms of additively manufactured porous biomaterials: Effects of porosity and type of unit cell. *Journal of the mechanical behavior of biomedical materials*, 50:180–191, 2015.

[8] I Ullah, M Brandt, and S Feih. Failure and energy absorption characteristics of advanced 3d truss core structures. *Materials & Design*, 92:937–948, 2016.

[9] Go Print 3D. 3d print master pro pla-n by filkemp. in: Go Print 3D Website (2020), https://www.goprint3d.co.uk/filkemp-pla-n.html Accessed 2020-12-11.

[10] A Standard. C393–00. standard test method for flexural properties of sandwich constructions, 2000.